Characteristic Parameters of Drift Vortices Coupled to Alfvén Waves in an Inhomogeneous Space Plasma

David Sundkvist* and Stuart D. Bale

Space Sciences Laboratory, University of California, Berkeley, 7 Gauss Way, Berkeley, California 94720, USA
(Received 7 February 2008; published 4 August 2008)

We present detailed measurements of ion scale vortices of drift type coupled to Alfvén waves in an inhomogeneous and collisionless space magnetoplasma. The two free parameters of a dipolar vortex, intensity and spatial radius, are measured. The vortices are driven by a strong density gradient on a boundary layer with scale size of the same order as the vortex diameter. Observations of vortices off the gradient show that symmetry-breaking conditions in a real inhomogeneous plasma can lead not only to cross-field but also to cross-boundary anomalous transport of particles and energy.

One outstanding problem for laboratory and experimental plasmas for fusion research is the observed transport of plasma across a confining magnetic field [1]. The best candidate to explain so-called cross-field anomalous transport is related to the presence of low-frequency drift waves and coherent structures [1–5]. Drift modes may be caused by pressure gradient driven instabilities due to inhomogeneities in plasma density and/or temperature. Conditions similar to a laboratory plasma are frequently found at boundary layers in astrophysical and space plasmas [6].

The basic model equation for low-frequency drift waves in strongly magnetized and inhomogeneous plasma is the Hasegawa-Mima equation (HME) [7], which admits solutions describing both (linear) drift waves as well as (nonlinear) localized coherent vortex structures of various types.

In a microphysical picture, a vortex is formed when energy is fed into a perturbation which can grow strong enough that self-trapping can occur, due to a nonlinearity of vector type. In an electrostatic vortex in a magnetized plasma $\mathbf{B}_0 = B_0\hat{\mathbf{z}}$, there is a surplus of charge on a field line. The strong radial electric field cannot neutralize the charge accumulation since the dominant convective vectorial velocity $\mathbf{v}_E = \mathbf{E} \times \mathbf{B}/B^2$ is directed in the azimuthal direction, causing the particles to circulate. Hence the vorticity $(\nabla \times \mathbf{v}_E)_{\parallel} = -\nabla_{\perp}^2 \phi/B\hat{\mathbf{z}} \neq 0$, which shows that drift modes are essentially vortex modes. In contrast, the mobility of the electrons in the direction along the magnetic field will allow currents $j_{\parallel}$ to flow in the case of an uneven charge distribution.

Alfvén waves are low-frequency electromagnetic transverse perturbations traveling along the magnetic field lines and are fundamental to large-scale energy transport in space, astrophysical, and laboratory plasmas [8]. A transverse magnetic perturbation is according to Ampere's law $\nabla \times \mathbf{B} = \mu_0\mathbf{j} + 1/c^2\partial\mathbf{E}/\partial t$ equivalent to a parallel current $j_{\parallel}$. This provides a natural coupling between an electrostatic vortex and an Alfvén wave. These more general vortices are denoted (drift-)Alfvénic vortices and are characterized by both an electrostatic potential ϕ as well as the parallel component of the magnetic vector potential $A_{\parallel}$ [9–15].

In this Letter, we use the collisionless magnetized space plasma in the terrestrial magnetosphere as a plasma laboratory and present the most detailed *in situ* measurements of drift vortices in inhomogeneous plasma to date. In particular, we determine the two free parameters of a particularly strong dipolar (modon) vortex, the potential strength and the vortex radius, using *in situ* multipoint measurements in a physically correct coordinate system for the first time.

We consider low-frequency fluctuations $\omega \ll \omega_{ci}$ in a strongly magnetized plasma $m_e/m_i \ll \beta \ll 1$, where $\omega_{ci} = qB/m_i$ is the ion gyrofrequency and β is the ratio of thermal to magnetic pressure. The low-frequency motion allows the use of the quasineutrality condition $n_i \approx n_e$ and the drift approximation for the perpendicular ion motion. The ion motion parallel to the ambient magnetic field $\mathbf{B}_0 = B_0\hat{\mathbf{z}}$ (ion sound waves) can be neglected due to a parallel phase velocity $v_{\text{th},i} \ll \omega/k_z \ll v_{\text{th},e}$. This is the parameter regime where linear drift waves are unstable and can grow due to a free energy source such as a pressure gradient. The inhomogeneity is assumed to be along $\hat{\mathbf{x}}$. The perpendicular electric field is purely potential $\mathbf{E}_{\perp} = -\nabla_{\perp}\phi$, while the parallel electric field and the magnetic field involve the parallel component of the magnetic vector potential $A_{\parallel}$. We get $\mathbf{E}_{\parallel} = -\hat{\mathbf{z}} \cdot \nabla\phi - \partial A_{\parallel}/\partial t$ for the electric field and $\mathbf{B} = \mathbf{B}_0 + (\nabla A_{\parallel}) \times \mathbf{B}_0/B_0$ for the magnetic field, where we have assumed $\delta\mathbf{B} \ll \mathbf{B}_0$.

From the two-fluid equations in the drift approximation, a set of nonlinear equations describing low-frequency drift waves (e.g., [9–15]) can be derived, describing the nonlinear evolution of drift-Alfvén waves as well as electrostatic drift waves, generalizing the electrostatic HME.

The HME and its electromagnetic generalization contain the ion gyroradius at electron temperature as a natural length scale $\rho_s = c_s/\omega_{ci}$ (it acts as the normalization unit length), where the sound speed is $c_s = \sqrt{T_e/m_i}$. The full system of equations, as well as the electrostatic HME,

admits localized coherent vortex solutions of Larichev-Reznik (dipolar, modon) type [16], as well as monopolar and tripolar vortices and vortex chains (e.g., [9–14]). A further generalization valid for scale sizes of the resulting dipolar vortices comparable to the Larmor radius was recently carried out [15]. These theoretical results are in accord with our observations as discussed below.

We now present observations of vortex structures consistent with the above-mentioned equations and their solutions, by the multispacecraft Cluster mission [17] from the cusp region of the terrestrial magnetosphere. The multipoint measurements make it possible to separate temporal and spatial phenomena, allowing us to determine the normal to the density gradient, construct a spatial scale, find the vortex potential, and calculate the current densities. The main plasma parameters are summarized in Table I and are seen to agree with the conditions for the electrostatic and Alfvénic drift modes summarized above. For an overview of the overall geophysical conditions associated with the cusp, see the papers on a previously reported cusp crossing [18] where vortices were detected [6].

On 6 April 2004 around 01:59:10 UT, the Cluster spacecraft were on an outbound trajectory entering a tailward boundary to the high-altitude cusp region. Figure 1(a) shows how the four spacecraft encounter a boundary layer with a strong density gradient. The density is calculated from the spacecraft potential [19]. The electric and magnetic fields have been decomposed into a field-aligned coordinate (FAC) system, with components displayed in Figs. 1(b)–1(f). The unit vectors of the FAC system are $\hat{\mathbf{z}} = \mathbf{B}_0/|\mathbf{B}_0|$ and $\hat{\mathbf{y}} = \hat{\mathbf{z}} \times \nabla n_e/|\nabla n_e|$, respectively, with $\hat{\mathbf{x}} = \hat{\mathbf{y}} \times \hat{\mathbf{z}}$ completing the right-handed system. Then $\{\hat{\mathbf{x}}, \hat{\mathbf{y}}\}$ spans the plane perpendicular to $\mathbf{B}_0$, with $\hat{\mathbf{z}}$ field aligned and $\hat{\mathbf{x}}$ pointing mostly along the density gradient. The $\mathbf{B}_0$ where $\mathbf{B}_0/|\mathbf{B}_0| = (-0.40, -0.02, -0.92)$ geocentric solar ecliptic (GSE) was determined by applying a running average of 3 s, which is about 8 times the proton gyroperiod. The density gradient normal direction $\hat{\mathbf{n}} = \nabla n_e/|\nabla n_e| = (-0.29, 0.96, 0.03)$ GSE and its velocity $v_{\text{gradient}} = 33$ km/s were found by assuming that it is a planar structure and using the time of crossing of the four spacecraft, together with their locations in space [20]. This

allows us to express the field quantities in the physically relevant coordinate system, proportional to (∇n_e, $\mathbf{B}_0 \times \nabla n_e$, $\mathbf{B}_0$), only possible due to the multipoint measurements and not previously done. Associated with the density gradient is a thin current sheet, visible in Fig. 1(f), which shows the parallel component of the ambient magnetic field. This current sheet is observed on all four spacecraft and provided an independent calculation of the gradient agreeing with the density measurement.

The FAC component measured by $C2$ pointing mostly along the gradient ($\hat{\mathbf{x}}$) is displayed in Fig. 1(b). We observe a strong, 160 mV/m peak to peak, tripolar electric field signature directly on the density gradient (highlighted in blue, hereafter referred to as vortex 1). We note, in particular, that the scale size of the structure r_0 is directly determined by the scale of the density gradient $r_0 \sim L$; cf. the red line in Fig. 1(a). Here $L = |\kappa|^{-1} = |-n'/n_0|^{-1}$ is the inhomogeneity scale size. This is contrary to the normal theoretical assumption $r_0 \ll L$. Below, we show that $r_0 = L/2$, where r_0 is the vortex radius. This signature of 1 s duration is the single strongest electric field signal during more than 1.5 h of data in the cusp. A tripolar electric field is a signature of a dipolar potential structure. Below, we show how this electric field is consistent with trapped particles in a drift vortex of dipolar (modon) type. The second highlighted patch (hereafter referred to as vortex 2) in Fig. 1 shows another vortex, now visible in the transverse electric field component. This dipolar electric field is consistent with either (1) a crossing of a dipolar vortex on the side of the vortex center or (2) a monopolar vortex. The data do not allow this ambiguity to be resolved for vortex 2. We note that this vortex is also observed in conjunction with a density inhomogeneity [red line in Fig. 1(a)]. The density topology for vortex 2 more resembles a cavity than a gradient and could possibly be self-consistently produced by the self-interacting spatially localized fields.

Both vortices are observed simultaneously with a strong and localized Alfvénic perturbation, with the perpendicular components of the magnetic field displayed in Figs. 1(d) and 1(e). By using the magnetic field and the velocity obtained above, the current density can be calculated from Ampere's law by neglecting the displacement current and assuming that the structures are convected past the spacecraft. We note that the peaks in both the transverse current as well as the parallel current [Figs. 1(g) and 1(h)] coincide with the location of the vortex structures visible in the electric field. We speculate that the parallel current is carried by field-aligned electrons in the shear Alfvén wave, which couples to the drift vortex mode as explained above. The transverse current (calculated from the parallel magnetic field) is consistent with a diamagnetic current sheet formed by the relative drift motion of electrons and ions caused by the density (pressure) gradient $\mathbf{j}_d = en(\mathbf{v}_{Di} - \mathbf{v}_{De})$, where $\mathbf{v}_D = -\nabla p \times \mathbf{B}/(qnB^2)$. Inserting numbers from Table I for the first highlighted area (location of

TABLE I. Characteristic plasma parameters in the cusp and derived vortex related parameters.

Quantity	Value	Quantity	Value
n_e [cm^{-3}]	2	v_A [km/s]	2600
T_i [eV]	300	c_s [km/s]	100
T_e [eV]	100	$v_{\perp,\text{gradient}}$ [km/s]	33
$|\mathbf{B}_0|$ [nT]	170	$v_{d,e}$ [km/s]	12
β	0.01	$v_{\text{th},e}$ [km/s]	5930
f_{ci} [Hz]	2.6	$v_{\text{th},i}$ [km/s]	240
ρ_s [km]	8	r_0 [ρ_s]	3
λ_i [km]	160	$\phi_{\max}$ [V]	400–550
$L = |\kappa|^{-1}$ [km]	50		
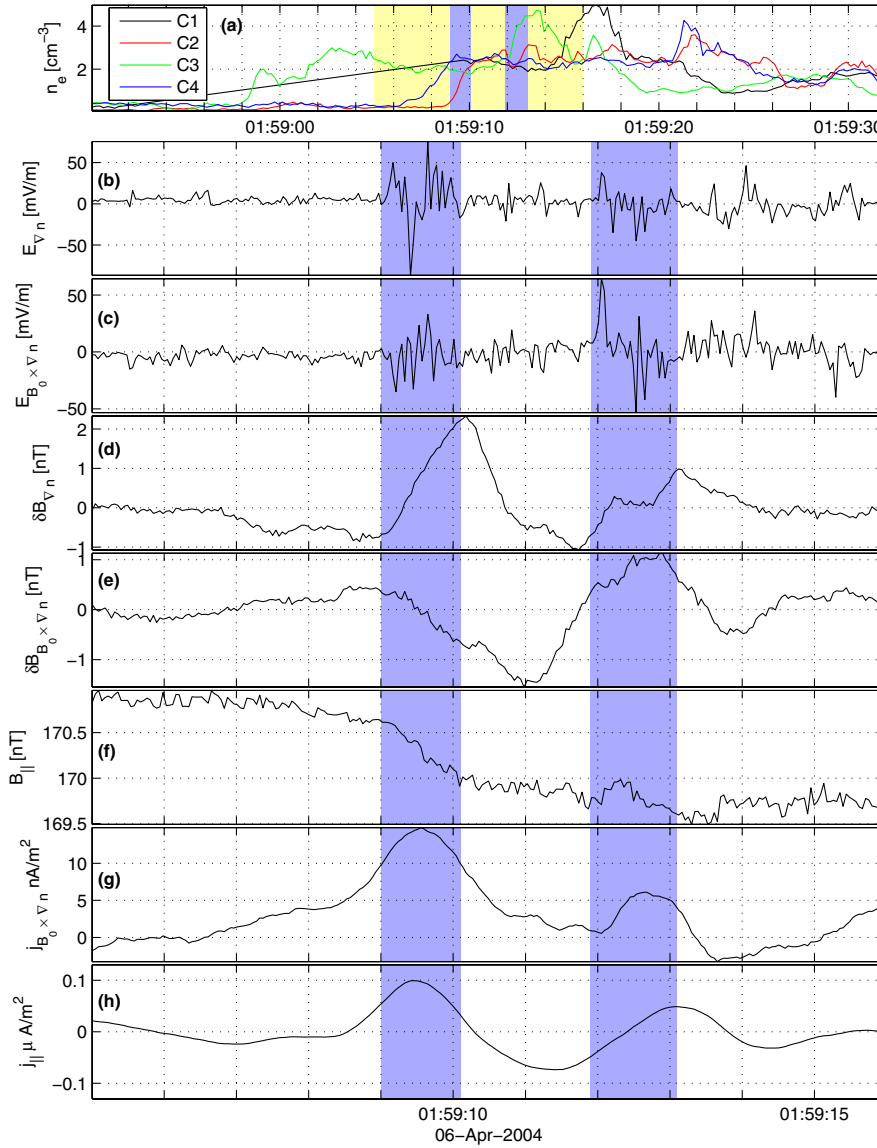
FIG. 1 (color online). Observations of drift vortices on a density gradient and coupled to an Alfvén wave, by the Cluster multispacecraft in the cusp region of the magnetosphere. See main text for a description of the coordinate system used. (a) shows four-spacecraft data, while (b)–(h) show data from $C2$. (a) Electron density showing the gradient. (b) Electric field perpendicular to the ambient magnetic field and along the density gradient. (c) Electric field perpendicular to the density gradient. (d) Perpendicular magnetic field along the density gradient. (e) Perpendicular magnetic field transverse to the gradient. (f) Parallel magnetic field. (g) Perpendicular current density. (h) Parallel current density. Note the different units for the current panels.

vortex 1), we get $j_D = 10$ nA/m^{-2}, in accord with the measured current density in Fig. 1(g).

We now determine the spatial size and calculate the strength of the potential field, the two free parameters for a dipolar vortex. Figure 2 shows a map of how spacecraft $C2$ and $C4$ cross vortex 1 in the plane perpendicular to the ambient magnetic field; compare with Fig. 1(b). The other two spacecraft are located outside the map. Here we have used the position of the spacecraft in the FAC-∇n_e system and assumed perpendicular convection using the velocity from four-spacecraft timing. From the analysis represented in Fig. 2, we get the vortex radius $r_0 \approx 24$ km $= 3\rho_s$, indicated by a yellow circle. We note that these scale sizes are in reasonable accord with the theoretical result that vortices should be found near the minimum vortex impedance [15].

To determine the potential strength (vortex intensity), we integrate the perpendicular electric field along the spacecraft trajectory (which is also in the perpendicular

plane). The result for vortex 1 is displayed in Fig. 3. We find $|\phi_{\max}| \sim 400$–550 V. The potential distribution in Fig. 3 is mainly dipolar, with an asymmetry due to the larger electric field on one side of the vortex, making it almost resemble a tripolar vortex [21]. This asymmetry could be due to, e.g., an inclination α of the vortex symmetry axis to $\mathbf{B}_0$, the intrinsic group velocity being comparable to the convection speed of the plasma, or the fact that the structure is a semitripolar vortex.

We now show that the critical amplitude and hence the trapping condition are fulfilled. For vortex 1, we get from Fig. 3 and Table I the dimensionless nonlinearity $\tilde{\phi} = e\phi/T_e \approx 5$. The angular rotation frequency inside the potential field is

$$\Omega_E = \frac{v_\theta}{r} = \frac{1}{rB_0}\frac{\partial\phi}{\partial r}. \quad (1)$$

With values from Table I, we get for an approximate shape of a potential maximum $\phi = \phi_{\max}(1 - r^2/r_0^2)$ the angular
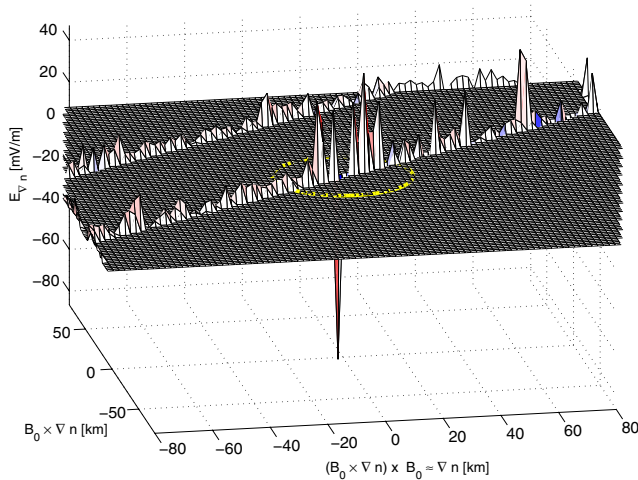
FIG. 2 (color online). Spacecraft trajectories and electric field from *C*2 (lower) and *C*4 (upper) in the $(\nabla n_e, \mathbf{B}_0 \times \nabla n_e)$ plane. The center of the coordinate system is the instantaneous position of *C*2 at the time of maximum absolute amplitude of $E_{\nabla n}$. The yellow circle indicates the vortex size, with an inferred vortex radius of $r_0 \approx 24$ km $= 3\rho_s$.

frequency $|\Omega_E| = 10$ s^{-1} and the vortex turnover time $T = 2\pi/\Omega_E = 0.6$ s. Comparing the angular frequency with the characteristic frequency for a (linear) drift wave $\omega^* = (k_y v_d)/(1 + k^2 \rho_s^2) \approx 0.6$ s^{-1}, we get $\Omega_E \gg \omega^*$. Hence the particle motion in the strong potential field is dominated by the rotational vortex flow, and the self-trapping condition is fulfilled.

The observations show that the vortices are formed on density gradients with a scale size twice the vortex radius but are also observed off the gradient. A similar result was found in a lab plasma [22], where coherent structures denoted "blobs" and "holes" were observed on a density gradient of similar scale size as the structures. In an idealized theoretical framework, a dipolar vortex has a linear
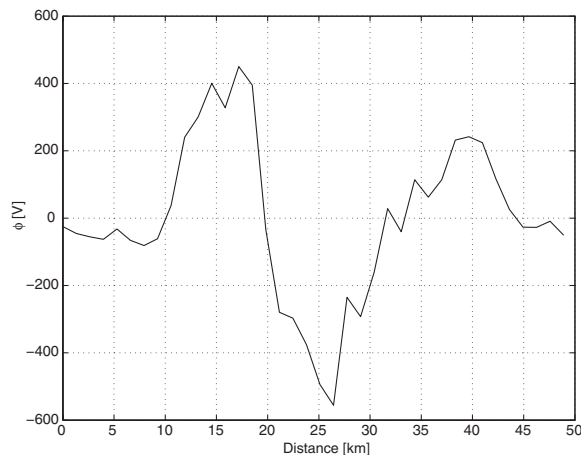
FIG. 3. Estimate of the electrostatic potential ϕ for vortex 1 integrated from the electric field perpendicular to the ambient magnetic field and along the spacecraft trajectory.

momentum in a direction perpendicular to both the ambient magnetic field as well as the density inhomogeneity, causing cross-field transport. In a real plasma, such as presented in this Letter, the ideal symmetry conditions are broken which can lead to cross-boundary (momentum component in the ∇n direction) as well as cross-field transport of particles and energy. A quantitative estimate of anomalous convective transport due to particle trapping in drift vortices with consequences for space boundary environments will be published elsewhere.

*sundkvist@ssl.berkeley.edu

[1] W. Horton and A. Hasegawa, Chaos **4**, 227 (1994).
[2] W. Horton, Phys. Fluids B **1**, 524 (1989).
[3] W. Horton, Rev. Mod. Phys. **71**, 735 (1999).
[4] J. J. Rasmussen, J. P. Lynov, J. S. Hesthaven, and G. G. Sutyrin, Plasma Phys. Controlled Fusion **36**, B193 (1994).
[5] G. Serianni *et al.*, Plasma Phys. Controlled Fusion **49**, B267 (2007).
[6] D. Sundkvist, V. Krasnoselskikh, P. K. Shukla, A. Vaivads, M. André, S. Buchert, and H. Rème, Nature (London) **436**, 825 (2005).
[7] A. Hasegawa and K. Mima, Phys. Fluids **21**, 87 (1978).
[8] K. Stasiewicz *et al.*, Space Sci. Rev. **92**, 423 (2000).
[9] V. M. Chmyrev, S. V. Bilichenko, O. A. Pokhotelov, V. A. Marchenko, V. I. Lazarev, A. V. Streltsov, and L. Stenflo, Phys. Scr. **38**, 841 (1988).
[10] T. D. Kaladze, V. A. Marchenko, O. A. Pokhotelov, and V. I. Petviashvili, Plasma Phys. Controlled Fusion **29**, 589 (1987).
[11] P. K. Shukla, M. Y. Yu, and R. K. Varma, Phys. Lett. **109A**, 322 (1985).
[12] A. B. Mikhailovskii, V. P. Lakhin, G. D. Aburdzhaniya, L. A. Mikhailovskaya, O. G. Onishchenko, and A. I. Smolyakov, Plasma Phys. Controlled Fusion **29**, 1 (1987).
[13] J. Liu and W. Horton, J. Plasma Phys. **36**, 1 (1986).
[14] V. I. Petviashvili and O. A. Pokhotelov, *Solitary Waves in Plasmas and in the Atmosphere* (Gordon and Breach, New York, 1992).
[15] O. G. Onishchenko, V. V. Krasnoselskikh, and O. A. Pokhotelov, Phys. Plasmas **15**, 022903 (2008).
[16] V. D. Larichev and G. M. Reznik, Dokl. Akad. Nauk SSSR **231**, 1077 (1976).
[17] C. P. Escoubet, R. Schmidt, and M. L. Goldstein, Space Sci. Rev. **79**, 11 (1997).
[18] D. Sundkvist *et al.*, Ann. Geophys. **23**, 983 (2005).
[19] A. Pedersen, P. Décréau, C.-P. Escoubet, G. Gustafsson, H. Laakso, P.-A. Lindqvist, B. Lybekk, A. Masson, F. Mozer, and A. Vaivads, Ann. Geophys. **19**, 1483 (2001).
[20] G. Paschmann and P. W. Daly, *Analysis Methods for Multi-Spacecraft Data* (ESA, Noordjwick, The Netherlands, 1998).
[21] D. Jovanović, F. Pegoraro, and J. J. Rasmussen, J. Plasma Phys. **60**, 383 (1998).
[22] T. A. Carter, Phys. Plasmas **13**, 010701 (2006).